Available online at www.sciencedirect.com

ScienceDirect

Procedia Structural Integrity 78 (2026) 222–229

Structural Integrity Procedia

www.elsevier.com/locate/procedia

XX ANIDIS Conference

A novel slip-friction connector for seismic applications in timber structures: analytical and experimental investigation

Matteo Pelliciari[a,*], Angelo Aloisio[b], Roberto Tomasi[c], Lars Vidar Jakobsen Næsse[c], Francesco Boggian[c], Pasqualino Gualtieri[b]

[a]*DIEF, Department of Engineering "Enzo Ferrari", via P. Vivarelli 10, 41125 Modena, Italy*
[b]*Department of Civil, Construction-Architectural and Environmental Engineering, Università degli Studi dell'Aquila, L'Aquila, 67100, Italy*
[c]*Faculty of Science and Technology, Norwegian University of Life Sciences, As, Norway*

Abstract

Slip-friction connectors are increasingly recognized as an effective strategy for enhancing the seismic performance of structures. Conventional solutions, however, commonly rely on bolt pretension to activate frictional resistance, which may lead to drawbacks such as preload losses over time, installation challenges, and concerns regarding long-term reliability. To overcome these limitations, this study proposes an innovative slip-friction connector that replaces bolt pretension with an elastic restoring force provided by a precompressed spring. The mechanical behavior of the proposed device is investigated through analytical modeling and experimental testing. An analytical solution is developed based on equilibrium equations, capturing the interaction between frictional sliding and elastic restoring effects in the force-displacement response. Cyclic tests are performed to validate the model and assess the energy dissipation capacity of the connector. Experimental results show excellent agreement with the analytical predictions, confirming the robustness of the proposed formulation. The findings of this study suggest that the proposed connector offers a promising solution for seismic applications in timber structures, with particular reference to cross-laminated timber (CLT) panels. In this context, the device may serve as an alternative to conventional connections, such as hold-downs, providing an efficient and tunable energy dissipation mechanism. The compact design, combined with the possibility of tailoring the mechanical response through spring stiffness adjustment, offers significant versatility for implementation in timber construction. Moreover, the simplicity of the analytical model ensures its practical applicability for design and engineering purposes.

Keywords: Frictional slip mechanisms; Analytical approach; Experimental testing; Wooden structural elements; Cyclic behavior.

* Corresponding author. Tel.: +393334858333.
E-mail address: matteo.pelliciari@unimore.it

2452-3216
10.1016/j.prostr.2025.12.029

1. Introduction

Slip-friction connectors dissipate energy through controlled sliding between preloaded surfaces, ensuring hysteretic behavior under cyclic loads. Due to their simplicity and effectiveness, they are increasingly adopted in structural engineering for seismic protection, especially in steel and concrete systems (Du et al., 2021; Jaisee et al., 2021; Dal Lago et al., 2017; Lu et al., 2023).

Recent research explores their use in timber engineering, where traditional mechanical fasteners often degrade under repeated loading, leading to reduced performance and difficult repair (Ceccotti et al., 2013; Zhang et al., 2021; Pei et al., 2016; Boggian et al., 2022). CLT panels and timber frame structures are commonly assembled using dry joints with metal fasteners, such as in hold-down systems, due to their low cost and ease of installation. Nevertheless, these conventional connections exhibit considerable deterioration when subjected to repeated cyclic loading, resulting in reduced stiffness, strength, and ductility over successive seismic events (Aloisio et al., 2022; Gavric et al., 2015). Furthermore, once damaged, these connections are challenging to repair or replace. In light of this, friction-based devices offer a promising alternative, showing improved energy dissipation and reusability compared to standard hold-downs (Loo et al., 2014; Hashemi and Quenneville, 2020; Hegeir et al., 2024).

Despite their potential, conventional slip-friction systems relying on bolt pretension face practical challenges: complex installation, preload loss over time, and surface wear, all of which may compromise performance (Golondrino et al., 2019). To overcome these issues, this study investigates an innovative slip-friction connector that uses a spring to generate normal force, eliminating the need for bolt pretension. The concept draws inspiration from the approach presented in (Dal Lago et al., 2021), applying the preload through a precompressed spring, with all components integrated within a hollow cylinder. The device is compact, versatile, and tunable in terms of stiffness and energy dissipation, making it suitable for seismic applications across various structural systems.

This work presents the device design, experimental testing, and an analytical model that captures its cyclic response. The proposed model is simple, closed-form, and validated against test data, providing a practical tool for engineering applications.

2. Experimental investigation

The proposed device, shown schematically in Fig. 1(a), consists of a hollow cylinder housing two hollow, wedge-shaped steel components, a precompressed spring, and a central bar. The lower wedge is fixed to the bar, while the upper wedge is free to move. The spring, compressed by tightening the lid, pushes the wedges together, activating friction at their inclined surfaces and at the lateral walls of the cylinder. When external displacement exceeds the frictional threshold, the wedges slide against the lateral walls, producing a stick-slip response with hysteretic energy dissipation. The spring provides an elastic restoring force, enabling the device to recover its initial configuration and sustain cyclic force-displacement behavior. This mechanism makes it suitable as a passive energy dissipation system in structures subjected to cyclic loading.

The wedges have a height of 60 mm, an outer diameter of 32 mm, and an inner diameter of 21 mm. The shear plane of the wedges is inclined at 60 degrees. The cylindrical housing has a total height of 110 mm, an external diameter of 37.5 mm, an internal diameter of 32.5 mm, and a wall thickness of 2.5 mm. The central threaded rod, to which the lower wedge is rigidly connected, has a diameter of 14 mm. At the top of the cylinder, a threaded section of 11.5 mm is used to secure the lid, ensuring the preload on the spring and maintaining the correct positioning of the internal components.

Three specimens with different springs were assembled for quasi-static cyclic testing (Pelliciari et al., 2025b). The threaded rod was connected to the lower wedge, while the spring was placed on the upper wedge. This assembly was inserted into the cylindrical housing and enclosed by tightening the lid. The specimens differed only in the spring type: (a) S1 with two coil springs in series (stiffness: 25 N/mm); (b) S2 with a single coil spring (stiffness: 75 N/mm); and (c) DS with a Belleville-type disc spring (initial stiffness: 246.7 N/mm). Further details on the springs are provided in (Pelliciari et al., 2025a).

Cyclic tests were performed using a ZwickRoell Z1200ES testing machine (Fig. 1(b)). The base of the connector was fixed to the machine using four M10 bolts, while the top was connected via a custom anchorage system for controlled displacement application. The loading protocol included three loading–unloading cycles from zero to a

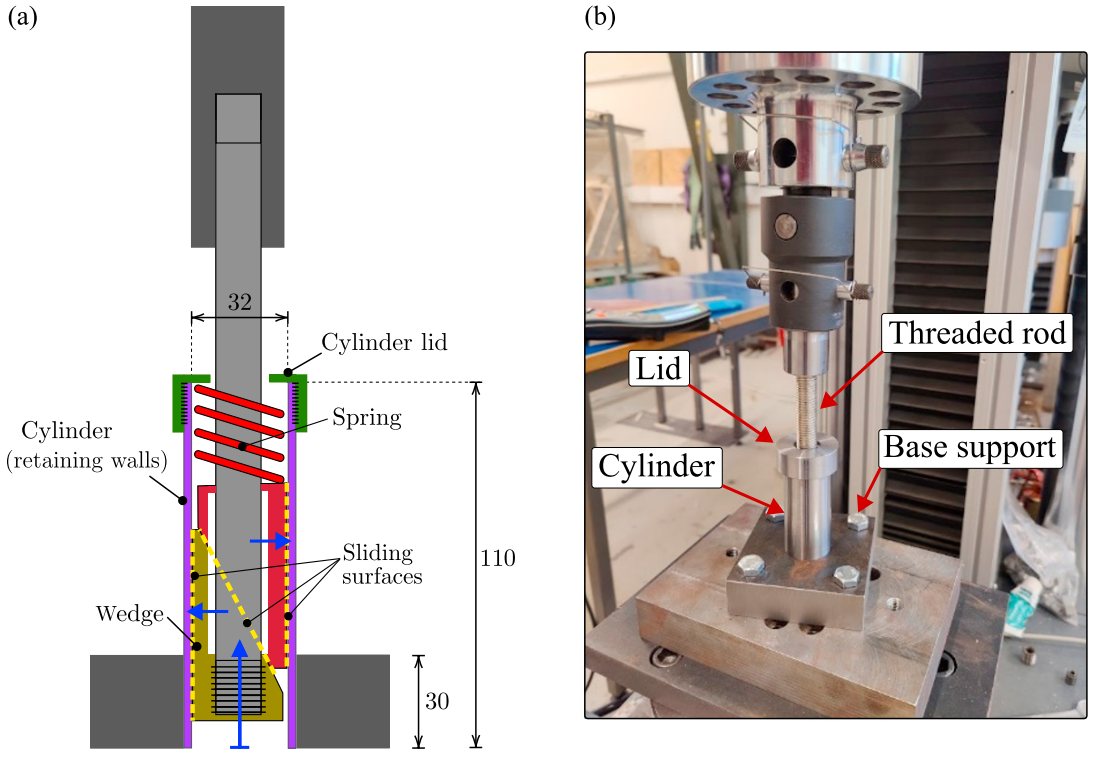

Fig. 1. (a) Schematic of the slip-friction device. The system comprises two wedges inside a hollow cylinder, preloaded by a compressed spring. The spring force presses the wedges against the inclined and lateral frictional interfaces. When the applied displacement exceeds the activation threshold, the wedges slide along the lateral walls, producing a stick-slip response with hysteretic force-displacement behavior due to combined elastic and frictional effects. Dimensions are in millimeters. (b) Experimental setup for quasi-static uniaxial cyclic tests used to evaluate the force-displacement response.

maximum displacement and back. A constant displacement rate of 5 mm/min ($\approx$ 0.08 mm/s) was applied in both directions to ensure quasi-static conditions. Prior to each test, the springs were preloaded to activate friction between the wedges and the cylinder walls in the initial configuration.

3. Analytical model

The proposed slip-friction device exhibits a characteristic stick–slip response under cyclic loading, governed by the interaction between frictional interfaces and the elastic restoring force of the preloaded spring. The device operates unidirectionally, with slipping phases occurring during both loading and unloading, as schematically illustrated in Fig. 2.

In the initial configuration, the spring is precompressed by a displacement $\tilde{x}_p$, which generates a preload force $F_p = F_s(\tilde{x}_p)$ that activates friction at both the inclined wedge surfaces and the lateral walls of the housing. When an external displacement x is applied, the system remains in stick phase until the applied force reaches the activation threshold at x_A, beyond which slip initiates. The force continues to grow as the spring is further compressed, and upon reversal of displacement direction, the system transitions to unloading, exhibiting hysteresis due to the directional dependence of friction forces.

The mechanical response is defined by four main parameters: wedge inclination angle θ, spring stiffness k, spring preload F_p, and friction coefficient μ. Assuming Coulomb friction (Márton and Lantos, 2009), the force–displacement

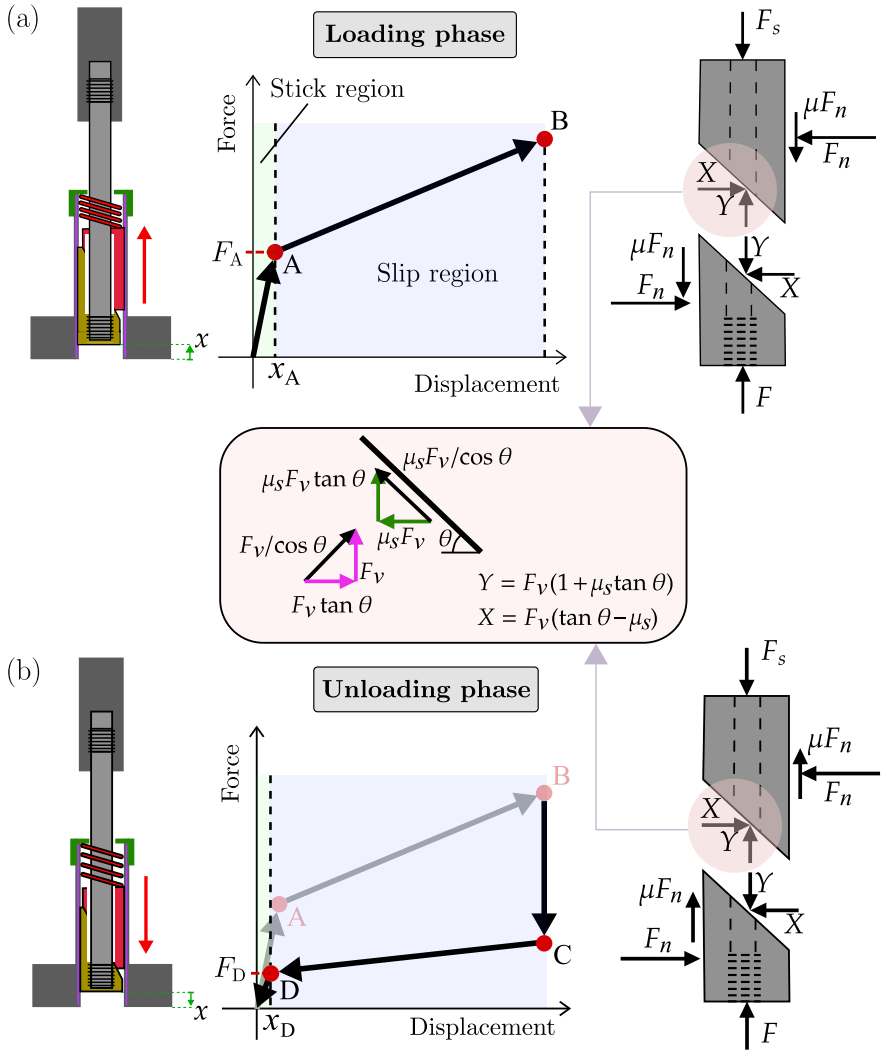

Fig. 2. Schematic of the slip–friction device under cyclic loading. Preload $\tilde{x}_p$ compresses the spring, pressing the wedges against the lateral walls and activating friction. (a) During loading, the device remains in stick region until $x = x_A$, then slips as the activation force is exceeded, with force increasing to point B. (b) Reversing displacement starts unloading, with a force drop to point C. The system returns to stick region at $x = x_D$.

relationship of the device is expressed as:

$$F = \begin{cases} k_A x, & \text{for } \dot{x} > 0 \text{ and } x \le x_A, \\ \psi F_s(\tilde{x}_p + x - x_A), & \text{for } \dot{x} > 0 \text{ and } x > x_A, \\ \psi^{-1} F_s(\tilde{x}_p + x - x_D), & \text{for } \dot{x} < 0 \text{ and } x > x_D, \\ k_D x, & \text{for } \dot{x} < 0 \text{ and } x \le x_D, \end{cases} \tag{1}$$

where the directional scaling factor ψ is defined as

$$\psi = \frac{1 - \mu_s\mu + (\mu_s + \mu)\tan\theta}{1 + \mu_s\mu + (\mu_s - \mu)\tan\theta}, \tag{2}$$

with μ_s being the static friction coefficient and μ the velocity-dependent friction coefficient, defined, for instance, by the Stribeck model $\mu = \mu_k + (\mu_s - \mu_k)e^{-\dot{x}/v_s}$, where $\dot{x} = dx/dt$, μ_k is the kinetic friction coefficient, and v_s is a reference velocity (Xiao et al., 2024). The stiffnesses k_A and k_D in the stick regions during loading and unloading are given by

$$k_A = k_n \left(\mu_s + \mu + \frac{1+\mu_s^2}{\tan\theta - \mu_s} \right), \tag{3}$$

$$k_D = k_n \left(\mu_s - \mu + \frac{1+\mu_s^2}{\tan\theta - \mu_s} \right), \tag{4}$$

where k_n accounts for the deformation of the lateral walls of the cylinder:

$$k_n = \frac{4\pi \bar{E} J_z \left(\tau h R^2 + J_z\right) \cot\theta}{\left(\pi^2 - 8\right)\tau h R^5 + \pi^2 J_z R^3}. \tag{5}$$

Here, R is the mean radius of the hollow cylinder, τ its wall thickness, h the height of the contact pressure area, and $\bar{E} = E/(1-\nu^2)$ the effective Young's modulus, with ν being Poisson's ratio. The term J_z is given by $J_z = -\tau h R^2 - h R^3 \ln\left((2R-\tau)/(2R+\tau)\right)$.

This model captures the asymmetric hysteretic force–displacement behavior of the device, combining frictional and elastic contributions. The reader is referred to (Pelliciari et al., 2025a) for full details of the model derivation.

3.1. Limit case of rigid retaining cylinder walls

In practice, the sliding displacements x_B (or x_C) are much larger than the stick-region amplitudes x_A and x_D, which stem from the deformation of the retaining walls. Assuming the cylinder behaves as rigid, these displacements can be neglected ($x_A, x_D \to 0$), and Eq. (1) simplifies to:

$$F = \begin{cases} \psi F_s, & \dot{x} > 0, \\ \psi^{-1} F_s, & \dot{x} < 0, \end{cases} \tag{6}$$

where $F_s = F_s\left(\tilde{x}_p + x\right)$ and ψ is defined in Eq. (2). This simplified model is practical, reducing both implementation effort and mathematical complexity, and can be readily applied in timber structures.

4. Results

The analytical model is validated against quasi-static cyclic tests on specimens S1, S2, and DS. The static friction coefficient is set to $\mu_s = 0.45$, consistent with typical steel-on-steel contact (Xie et al., 2000; Pijpers and Slot, 2020). The low test displacement rate (quasi-static) justifies the assumption $\mu \approx \mu_s$ in the model. Preload displacements $\tilde{x}_p$ and corresponding forces F_p are summarized in Table 1, along with other model parameters.

Figure 3 compares experimental force–displacement and energy curves (dashed lines) with model predictions from Eq. (1) (solid lines). The model captures well the cyclic behavior, including stiffness in both phases and activation forces. Even under the simplifying assumption of rigid retaining walls (Eq. (6)), predictions would remain accurate, as x_A and x_D are negligible compared to the sliding displacement.

The largest discrepancy appears in DS during unloading (Fig. 3(e)), likely due to higher variability and fewer repeated tests. Nonetheless, the model shows robust performance and good agreement overall, despite assumed rather

Table 1. Parameters of the analytical model and experimental setup for specimens S1, S2, and DS.

Parameter	Symbol	S1	S2	DS
Wedge angle	θ	60°	60°	60°
Static friction coefficient	μ_s	0.45	0.45	0.45
Spring stiffness (N/mm)	k	25	75	246.7
Preload displacement (mm)	$\tilde{x}_p$	9	5	3
Preload force (N)	F_p	225	375	675.5

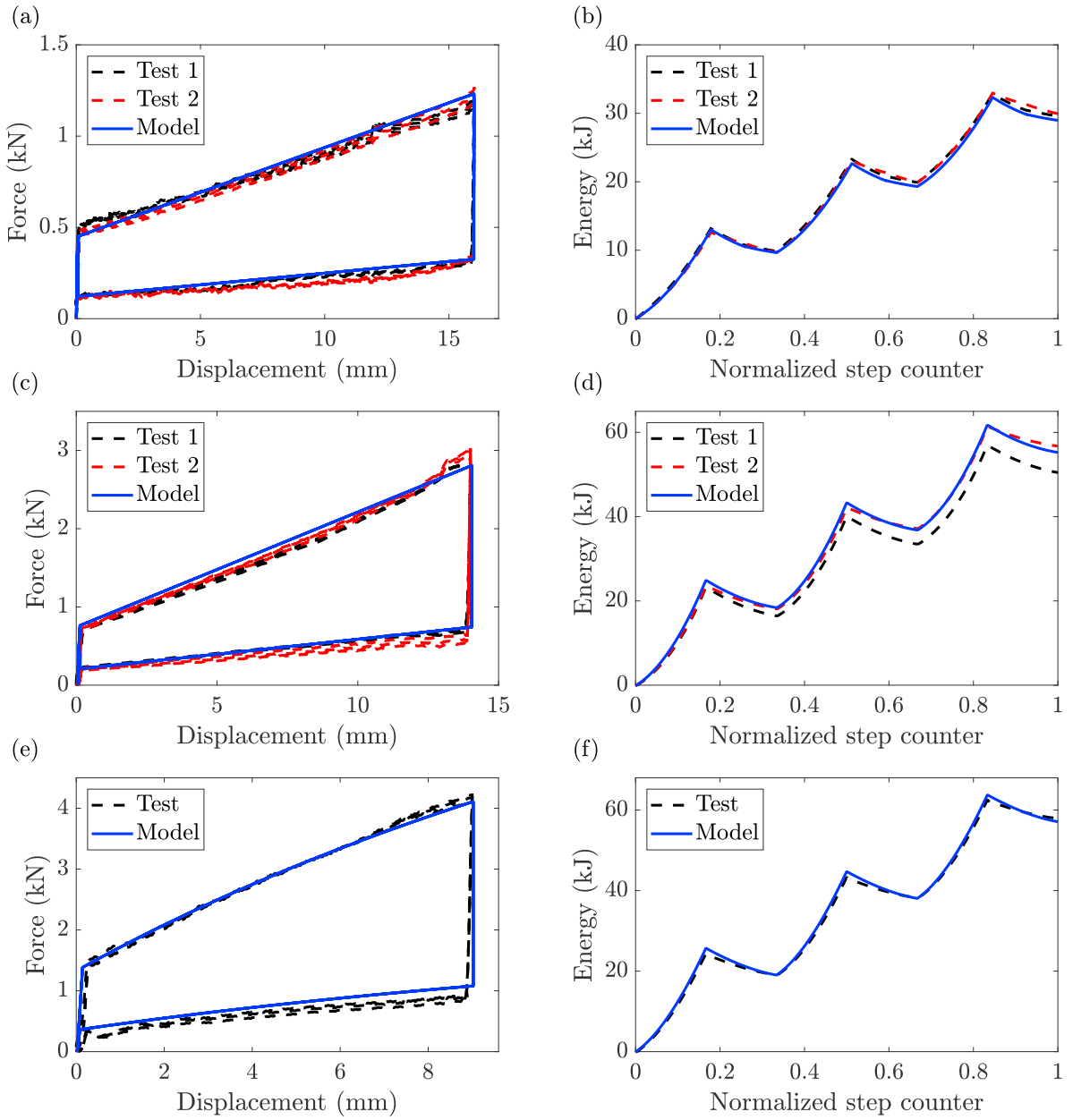

Fig. 3. Experimental (dashed) and analytical (solid) force–displacement and total input energy curves for specimens: (a,b) S1, (c,d) S2, and (e,f) DS.

than measured friction values. In summary, the proposed analytical model provides an effective and accurate representation of the cyclic response, demonstrating its validity for predicting the mechanical behavior of the slip–friction connector.

5. Conclusions

This study examined the mechanical behavior of a novel slip–friction connector for structural applications. The device addresses common limitations of conventional friction-based connections, such as preload loss, complexity, and limited long-term stability, by combining frictional sliding with an elastic restoring force from a spring, eliminating the need for bolt pretension. Analytical modeling and experimental testing were integrated to characterize its cyclic response and assess practical feasibility.

The analytical model, derived from equilibrium equations, provides a closed-form solution that accurately predicts the hysteretic behavior of the device. It captures the interplay between frictional slip and elastic restoring forces, and highlights the influence of design parameters on performance and energy dissipation. Its simplicity and accuracy make it suitable for engineering applications.

Experimental tests validated the model, showing strong agreement with predictions and confirming the stability, repeatability, and energy dissipation capacity of the device. The ability to tune its response by adjusting the spring, without altering the overall geometry, further enhances its versatility.

The results demonstrate the potential of the proposed connector as an effective alternative to traditional dissipative connections, particularly in timber structures, but also in other systems requiring controlled energy dissipation. Its advantages include ease of implementation, compact design, self-centering capability, and adaptability. Beyond structural engineering, the concept shows promise for applications in vibration mitigation, mechanical damping (e.g., aerospace and impact absorption), vehicle suspensions, and similar systems.

This study focused on quasi-static conditions. Future work will include a comprehensive dynamic experimental campaign and model refinements to capture advanced friction behavior, wear, and contact degradation. Further simulations under realistic cyclic excitations, such as seismic, harmonic, and impact loads, will also be conducted to explore broader applications.

Acknowledgements

This work was supported by the University of Modena and Reggio Emilia through the project “FAR Dipartimentale 2024-2025” (CUP E93C24000500005). Additional support was provided by the Italian Ministry of University and Research (MUR) through the research grant FISA-2022 “Earth-Tech” (CUP E93C24000250001).

References

Aloisio, A., Contento, A., Alaggio, R., Briseghella, B., Fragiacomo, M., 2022. Probabilistic assessment of a light-timber frame shear wall with variable pinching under repeated earthquakes. Journal of Structural Engineering 148, 04022178.

Boggian, F., Tardo, C., Aloisio, A., Marino, E.M., Tomasi, R., 2022. Experimental cyclic response of a novel friction connection for seismic retrofitting of RC buildings with CLT panels. Journal of Structural Engineering 148, 04022040.

Ceccotti, A., Sandhaas, C., Okabe, M., Yasumura, M., Minowa, C., Kawai, N., 2013. SOFIE project–3D shaking table test on a seven-storey full-scale cross-laminated timber building. Earthquake Engineering & Structural Dynamics 42, 2003–2021.

Dal Lago, B., Biondini, F., Toniolo, G., 2017. Friction-based dissipative devices for precast concrete panels. Engineering Structures 147, 356–371.

Dal Lago, B., Naveed, M., Lamperti Tornaghi, M., 2021. Tension-only ideal dissipative bracing for the seismic retrofit of precast industrial buildings. Bulletin of Earthquake Engineering 19, 4503–4532.

Du, X., Wang, Z., Liu, H., Liu, M., 2021. Research on seismic behavior of precast self-centering concrete walls with dry slip-friction connectors. Journal of Building Engineering 42, 102668.

Gavric, I., Fragiacomo, M., Ceccotti, A., 2015. Cyclic behaviour of typical metal connectors for cross-laminated (CLT) structures. Materials and structures 48, 1841–1857.

Golondrino, J.C.C., MacRae, G.A., Chase, J.G., Rodgers, G.W., Clifton, G.C., 2019. Asymmetric friction connection (AFC) design for seismic energy dissipation. Journal of Constructional Steel Research 157, 70–81.

Hashemi, A., Quenneville, P., 2020. Large-scale testing of low damage rocking cross laminated timber (CLT) wall panels with friction dampers. Engineering Structures 206, 110166.

Hegeir, O.A., Malo, K.A., Stamatopoulos, H., 2024. An innovative slip-friction moment-resisting connection using screwed-in threaded rods in cross laminated timber and steel coupling parts: An experimental study. Engineering Structures 318, 118654.

Jaisee, S., Yue, F., Ooi, Y.H., 2021. A state-of-the-art review on passive friction dampers and their applications. Engineering Structures 235, 112022.

Loo, W., Quenneville, P., Chouw, N., 2014. A new type of symmetric slip-friction connector. Journal of Constructional Steel Research 94, 11–22.

Lu, Y., Liu, Y., Wang, Y., Liu, J., Huang, X., 2023. Development of a novel buckling-restrained damper with additional friction energy dissipation: Component tests and structural verification. Engineering Structures 274, 115188.

Márton, L., Lantos, B., 2009. Control of mechanical systems with Stribeck friction and backlash. Systems & Control Letters 58, 141–147.

Pei, S., van De Lindt, J.W., Popovski, M., Berman, J.W., Dolan, J.D., Ricles, J., Sause, R., Blomgren, H., Rammer, D.R., 2016. Cross-laminated timber for seismic regions: Progress and challenges for research and implementation. Journal of Structural Engineering 142, E2514001.

Pelliciari, M., Aloisio, A., Tomasi, R., 2025a. Analytical and experimental study of a novel slip-friction connector for structural mechanics. European Journal of Mechanics-A/Solids 114, 105721.

Pelliciari, M., Sirotti, S., Aloisio, A., Tarantino, A.M., 2025b. Hyperelastic model for nonlinear elastic deformations of graphene-based polymer nanocomposites. International Journal of Solids and Structures 308, 113144.

Pijpers, R.J.M., Slot, H.M., 2020. Friction coefficients for steel to steel contact surfaces in air and seawater, in: Journal of Physics: Conference Series, IOP Publishing. p. 012002.

Xiao, Y., Wu, N., Wang, Q., 2024. Energy generation from friction-induced vibration of a piezoelectric beam. International Journal of Mechanical Sciences 280, 109648.

Xie, W., De Meter, E.C., Trethewey, M.W., 2000. An experimental evaluation of coefficients of static friction of common workpiece–fixture element pairs. International Journal of Machine Tools and Manufacture 40, 467–488.

Zhang, X., Isoda, H., Sumida, K., Araki, Y., Nakashima, S., Nakagawa, T., Akiyama, N., 2021. Seismic performance of three-story cross-laminated timber structures in Japan. Journal of Structural Engineering 147, 04020319.